Review of Scientific Instruments

Slow- and rapid-scan frequency-swept electrically detected magnetic resonance of MOSFETs with a non-resonant microwave probe within a semiconductor wafer-probing station

Cite as: Rev. Sci. Instrum. **90**, 014708 (2019); https://doi.org/10.1063/1.5053665
Submitted: 24 August 2018 . Accepted: 24 December 2018 . Published Online: 14 January 2019

Duane J. McCrory, Mark A. Anders, Jason T. Ryan, Pragya R. Shrestha, Kin P. Cheung, Patrick M. Lenahan, and Jason P. Campbell

Slow- and rapid-scan frequency-swept electrically detected magnetic resonance of MOSFETs with a non-resonant microwave probe within a semiconductor wafer-probing station

Cite as: Rev. Sci. Instrum. 90, 014708 (2019); doi: 10.1063/1.5053665
Submitted: 24 August 2018 • Accepted: 24 December 2018 •
Published Online: 14 January 2019

Duane J. McCrory,[1,2,a)] Mark A. Anders,[1,2] Jason T. Ryan,[1] Pragya R. Shrestha,[1,3] Kin P. Cheung,[1] Patrick M. Lenahan,[2] and Jason P. Campbell[1]

AFFILIATIONS

[1] Nanoscale Device Characterization Division, National Institute of Standards and Technology, 100 Bureau Drive, MS 8120, Gaithersburg, Maryland 20899, USA
[2] Engineering Science and Mechanics, Pennsylvania State University, 101 EES Building, University Park, Pennsylvania 16801, USA
[3] Theiss Research, La Jolla, California 92037, USA

[a)] Author to whom correspondence should be addressed: duane.mccrory@gmail.com

ABSTRACT

We report on a novel electron paramagnetic resonance (EPR) technique that merges electrically detected magnetic resonance (EDMR) with a conventional semiconductor wafer probing station. This union, which we refer to as wafer-level EDMR (WL-EDMR), allows EDMR measurements to be performed on an unaltered, fully processed semiconductor wafer. Our measurements replace the conventional EPR microwave cavity or resonator with a very small non-resonant near-field microwave probe. Bipolar amplification effect, spin dependent charge pumping, and spatially resolved EDMR are demonstrated on various planar 4H-silicon carbide metal-oxide-semiconductor field-effect transistor (4H-SiC MOSFET) structures. 4H-SiC is a wide bandgap semiconductor and the leading polytype for high-temperature and high-power MOSFET applications. These measurements are made via both "rapid scan" frequency-swept EDMR and "slow scan" frequency swept EDMR. The elimination of the resonance cavity and incorporation with a wafer probing station greatly simplifies the EDMR detection scheme and offers promise for widespread EDMR adoption in semiconductor reliability laboratories.

INTRODUCTION

Electrically detected magnetic resonance (EDMR) has become a powerful tool for investigating performance limiting defects in a wide variety of material systems.[1–7] EDMR has been shown to be far more sensitive than conventional electron paramagnetic resonance (EPR), detecting fewer than 100 spins;[8] however, it is comparatively underutilized to study point defects which control the performance and reliability of solid state electronics.[7,9–13] This is due, at least in part, to the experimental challenges associated with the EDMR measurement. Quite simply, typical EDMR sample preparation (wafer dicing, mounting, and fashioning of "resonator friendly" device electrical connections) is dictated by the conventional EPR experimental approaches. These specially prepared devices[8,14–16] conflict with the typical methods used in very large scale electrical device characterization (i.e., rapid wafer-level probing of voltages, currents, and impedances).

Most EDMR literature details experiments in which the fundamental components of a conventional EPR spectrometer are modified to allow for device current monitoring. These efforts are largely bound by the requirements of conventional EPR detection. Removal of the conventional resonator from the EDMR experiment eliminates cavity loading problems, provides better access to device electrical connections, and renders the microwave excitation/detection inherently broadband. Recent EDMR reports demonstrate the use of coplanar strip line antennas *in lieu* of the resonator[17] to introduce microwave magnetic fields. In this work, the strip line antenna structure is deposited directly on the device under test. Recent non-resonant antenna probe-based EPR reports provide similar demonstrations of non-resonant competence by simply positioning an antenna structure above the device in a scanned probe type arrangement.[18] Collectively, this work provides a path toward resonator-free EDMR measurements. However, the overall experimental approach (removal of the resonator) still relies heavily on the conventional spectrometer paradigm.

In an effort to change this paradigm, we report on the first demonstration of continuous-wave slow- and rapid-scan[19,20] frequency-swept EDMR measurements in a modified conventional wafer probing station. This effort utilizes a fixed annular shaped permanent magnet mounted above the wafer chuck, a non-resonant microwave "antenna" probe which can be positioned above the device under measurement, and up to four additional electrical probes for device biasing and current measurement. The capability of this approach is demonstrated via X-band continuous-wave frequency-swept EDMR measurements of the Si-vacancy defect present in SiC/SiO_2 field effect transistors (SiC is a wide bandgap material for use in high-power and high-temperature applications).[1–4] This Si-vacancy defect is observed in a variety of spin dependent recombination current modes. This includes SiC/SiO_2 interfacial recombination observed using both the bipolar amplification effect (BAE)[21] and spin dependent charge pumping (SDCP).[22] It also includes SiC source to substrate junction recombination observed in both the linear response slow-scan and rapid-scan regimes. In a final demonstration of utility, the position of the non-resonant microwave probe is varied to yield a somewhat crude spatially resolved EDMR measurement. This manuscript illustrates the first demonstration of a fully functional wafer-probing station capable of EDMR measurements of point defects that directly impact the performance and reliability of nominally prepared devices.

EXPERIMENTAL APPROACH

EDMR, like conventional EPR, requires the application of a large uniform magnetic field (B_0). In our apparatus, B_0 was realized by mounting an axially magnetized annular shaped NdFeB (neodymium) permanent magnet (grade = N52, outer diameter = 50.8 mm, inner diameter = 10 mm, and thickness = 50.8 mm) on a vertical translation stage above the wafer chuck. The translation stage is used for both coarse and fine magnet field adjustments. Figure 1(a) shows a photograph of the annular magnet mounted in the probe station. The annular shape provides an optical window for device and probe positioning while still providing fields sufficient for X-band EDMR operation (≈320 mT). As shown in Fig. 1(b), three-dimensional finite element calculations verify that this geometry results in a small but adequate region of uniformity

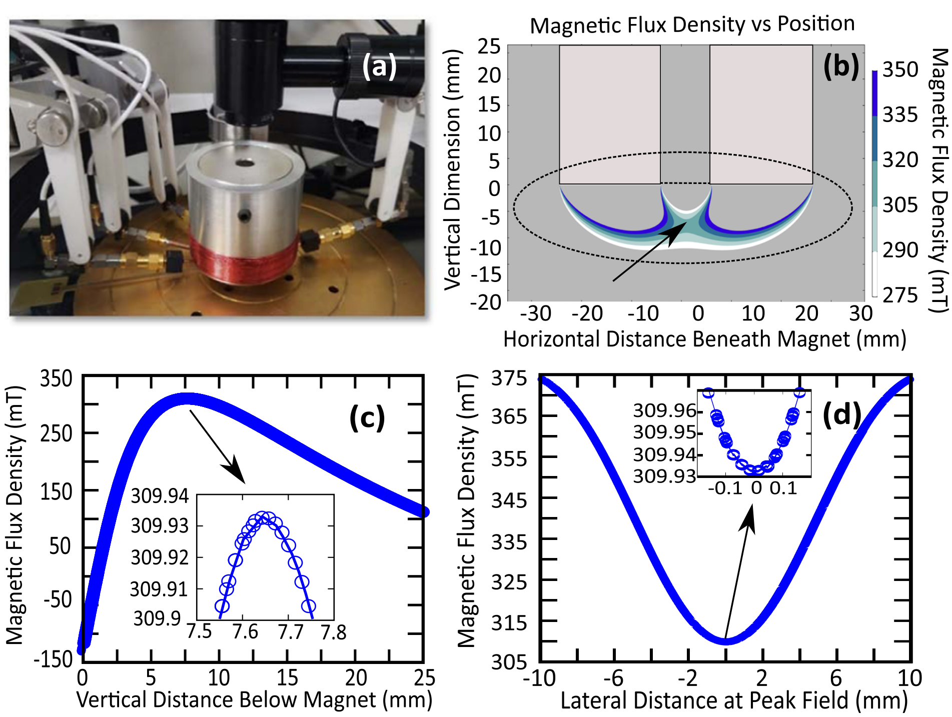

FIG. 1. (a) A photograph of the axially magnetized neodymium permanent magnet mounted above the wafer chuck. (b) A simulation of the magnetic flux density of the same permanent magnet. The region enclosed by the dotted oval indicates the region of higher magnetic flux density. The very center of that region is the area of uniformity where the EDMR samples are placed. (c) illustrates the calculated magnetic flux density versus vertical distance below the magnet. (d) illustrates the calculated magnetic flux density versus horizontal position below the magnet. The insets of (c) and (d) illustrate the "zoomed-in" view of vertical and horizontal uniformity within the peak of the magnetic flux density below the magnet.

approximately 7.5 mm from the bottom surface of the magnet. The region enclosed within the oval indicates the magnetic flux density versus position beneath the magnet. This is further illustrated by the Cartesian field uniformity plots shown in Figs. 1(c) and 1(d), which indicate 100 parts per million uniformity (30 μT over ≈200 μm diameter sphere). While the region of uniformity may seem exceedingly small when compared to conventional EPR magnetic field homogeneities, this region is far larger than the typical device dimensions probed in EDMR measurements. The region of uniformity is denoted with arrows in Figs. 1(b)–1(d). Considering that the majority of EDMR line widths are ≥0.3 mT, the magnetic field uniformity is adequate to accurately measure most EDMR spectra.

In a typical EDMR measurement, we ensure that the device is placed within the "EMDR sweet spot" by utilizing the fixed working distance (82 mm) of the microscope. First, we calibrate the magnetic field with a Hall probe placed on the surface of the wafer chuck. We can dial into the EDMR sweet spot by focusing the microscope on the surface of the Hall probe and then independently change the vertical position of the magnet with the attached micrometer. Once the field is calibrated to the maximum peak, we fix the micrometer settings. Next, the device under test is moved into the sweet spot, and the entire magnet/microscope apparatus is moved vertically until the surface of the device comes into focus. Lateral placement occurs in a similar fashion and uses the electrical probes as additional points of reference. This process occurs before each EDMR measurement.

The magnet dimensions were chosen for both the resulting field strength and maximization of the available space below the magnet opening (≈7.5 mm) for maneuvering the non-resonant microwave probe and electrical biasing probes. Each biasing probe uses a coaxial connection to minimize the electrical noise of the measurement.

In conventional EDMR experiments, the microwave magnetic field (B_1) is provided by using a microwave resonator, typically at X-band frequencies ($\upsilon \cong 9-10\,\mathrm{GHz}$). Unlike conventional EPR which involves detection of the reflected microwave power, EDMR detection involves a simple device current measurement. Detection of EPR in this fashion provides two distinct experimental advantages: (1) precise measurement of device currents is comparatively easier than the precise measurement of microwave power and (2) the EDMR measurements only observe defects which impact the device current. Identification of these electrically active defects is imperative for improving the performance of nanoscale devices. The simplest EDMR measurements involve spin dependent recombination (SDR) in a p-n junction. A small forward bias is applied to the junction which induces a recombination current in the depletion region. As discussed by Kaplan, Solomon, and Mott (KSM) in their seminal paper,[23] recombination is a spin dependent process. The spin interactions between a paramagnetic defect site and a charge carrier can alter the recombination rate. In general, a charge carrier cannot transition to the defect site if the defect-carrier pair is in the triplet configuration but is allowed if the pair is in a singlet configuration. Thus, only pairs in a singlet configuration can recombine. EPR increases the ratio of singlets to triplets by "flipping" the spin of the defect center. The flipping event occurs at the resonance condition which, in the simplest case of a free electron, is described by Eq. (1),

$$h\nu = g\mu_B B, \tag{1}$$

where h is Planck's constant, μ_B is the Bohr magneton, and in the simplest case of an isolated electron in a strong magnetic field of magnitude ($B \approx 350$ mT), $g_e = 2.0023$. In real material systems, the EPR response is most frequently dominated by two phenomena: spin-orbit coupling and electron-nuclear hyperfine interactions which modify Eq. (1) from the simplest case. Analysis of these interactions allows for direct information about the physiochemical nature of the defect surroundings.

In this study, B_1 was applied to the device under test by positioning a non-resonant shorted coaxial probe on the wafer surface, next to the device. The copper coaxial probe has an outer diameter of 508 μm and an inner conductor diameter of 50 μm. The inner conductor protrudes beyond the end of the probe ≈380 μm and is shorted to the outside of the coaxial line with a 38.1 μm diameter gold wire. In practice, this shorted non-resonant probe is realized in a process quite similar to those used to fabricate commercially available ground-signal-ground high speed wafer probes. These dimensions were chosen to simultaneously ensure sufficient B_1 uniformity beneath the probe and ample freedom to position the probe within the tight confines of a typical device layout. A thin coating of ethyl acetate (nail polish) was deposited on the loop of the microwave probe to limit any inadvertent electrical biasing that may occur when the probe is landed on the surface of the wafer. The probe must be placed on the wafer; otherwise, the probe vibrates above the device under test, which leads to a significant increase in the effective microwave coupling and subsequent electrical noise. This microwave probe is capable of handling at least 1 W of power and is rigid enough to allow contact with the surface of the device. The broadband nature of the probe is verified through (S_{11}) vector network analyzer measurements which reveal a flat frequency response (~0.5 dB variation) across the frequency sweep ranges (8-10 GHz) utilized in this study. The non-resonant microwave probe is mounted on a conventional wafer probe manipulator and can be independently positioned in concert with the electrical biasing probes. These probes bias the device under test and detect the EDMR currents. This experimental arrangement is illustrated in Figs. 2(a) and 2(b). The near-field microwave magnetic field emanating from the non-resonant antenna probe can be crudely understood by envisioning the magnetic field associated with the current traveling in the shorting wire [Fig. 2(c)]. In this case, one would anticipate that the magnetic field density would drop as the inverse of the radius, based upon the Biot-Savart law. This general behavior is verified using three-dimensional finite element simulations [Fig. 2(d)] for an input power of 1 W and provides a region near the short (lighter color) with relatively

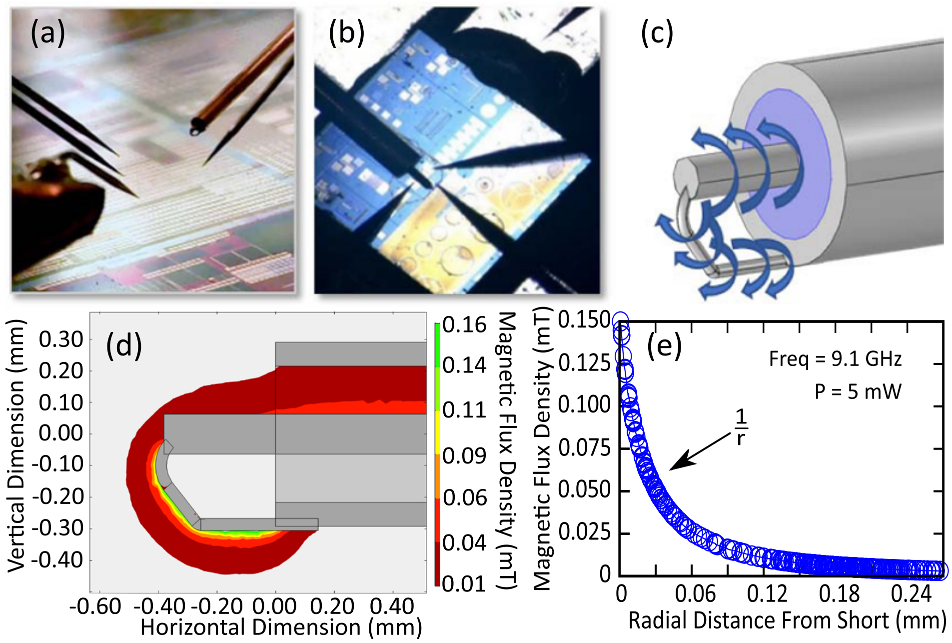

FIG. 2. (a) A photograph of the non-resonant coaxial probe and the custom electrical biasing probes. (b) An overhead photograph of all of the probes arranged near the device under test. (c) A cartoon illustration of the generated B_1 from the non-resonant coaxial probe. (d) The calculated magnetic flux density versus position around the non-resonant coaxial probe. The lighter regions closer to the loop indicate greater magnetic flux density. (e) The calculated magnetic flux density versus position below the non-resonant coaxial probe. Reprinted with permission from McCrory *et al.*, IEEE Trans. Device Mater. Reliab. **18**(2), 139 (2018). Copyright IEEE 2018.[32]

high B_1 [Fig. 2(e)]. Typically, in conventional EDMR measurements, the EDMR response is maximized when the spin system is driven into saturation via the application of a large B_1.[24] The non-resonant probe is capable of generating a small region wherein B_1 is at least orders of magnitude greater than a conventional TE_{102} cavity.[25] Therefore, the non-resonant microwave probe should have greater sensitivity in comparison with a conventional EDMR resonator over these small regions of excitation.

Using this antenna probe approach does, admittedly, lead to some B_1 intensity non-uniformities, especially with larger devices. However, since most modern device structures have active area depths <2 μm, B_1 is essentially uniform over the sample under investigation. It is also important to realize that the effective B_1 depth penetration can be controlled by changing the microwave input power (bounded only by the power limitations of the shorting wire). Armed with a somewhat crude understanding of the B_1 uniformity, lateral movement of the antenna probe across the surface of the device can provide rough spatial profiling.

This arrangement is also quite unusual in that B_0 is fixed (no sweep or modulation coils). Instead, the spectra are acquired by sweeping the frequency of the input microwave source. Frequency swept detection is nearly always avoided due to the steep experimental roadblocks arising from resonator detection and the common utilization of finely tuned microwave bridge circuits.[26] Considering that (1) the B_1 antenna probe is inherently broadband and (2) EDMR current detection only requires sufficient B_1 to saturate the spin system, this experimental approach benefits greatly from swept frequency measurements. Within this scheme, B_1 frequency and B_1 amplitude modulation are easily employed using most modern microwave sources. The non-resonant probe is also suitable for rapid frequency sweeps which, provided the relaxation times are amenable, can introduce signal to noise improvements due to passage effects.[19]

As mentioned above, these two essential EDMR components [permanent magnet (B_0) and antenna probe (B_1)] are integrated in a conventional wafer probing station, as schematically illustrated in Fig. 3. In this setup, wafer-level measurements across many devices can be achieved without any extra sample preparation (dicing, wire-bonding, etc.). This quite substantial simplification of sample preparation will allow the combination of EDMR and conventional device electrical characterization.

We have demonstrated the efficacy of this non-resonant EDMR measurement approach in 150 mm wafers with n-channel 4H-SiC metal oxide semiconductor field effect transistors (MOSFETs). These MOSFETs have a dominating performance limiting defect (Si-vacancy) with a corresponding spectrum with an EDMR linewidth of ~0.5 mT with a zero-crossing g-value of 2.0030.[27] The devices investigated in this study had two different gate sizes (100 μm × 100 μm and 250 μm × 4 μm) with a silicon dioxide thickness of 50 μm or 75 μm. Source-substrate junction spin dependent recombination current measurements were performed on both types of devices. The source-drain current (measured using BAE),[21] as well as the interface recombination current (measured via SDCP), were performed on the narrower channel devices (250 μm × 4 μm). The non-resonant measurements were compared with modulated and swept magnetic field electromagnet/resonator-based EDMR measurements using a conventional X-band EDMR spectrometer. All measurements were made at room temperature.

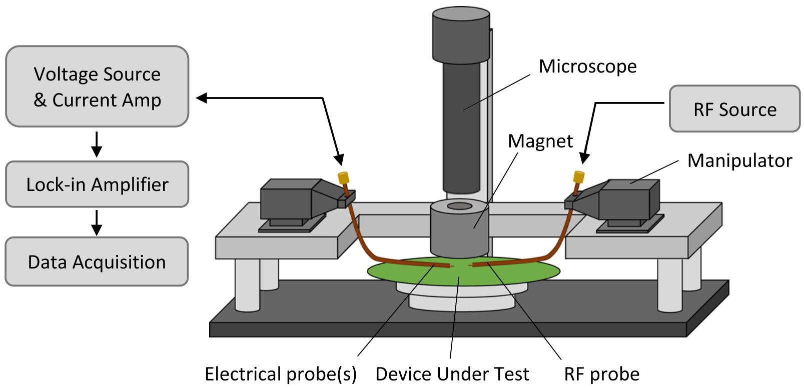

FIG. 3. A cartoon illustration of the key components for the wafer-level EDMR spectrometer.

RESULTS AND DISCUSSION

Spin dependent recombination

Figure 4 illustrates a comparison of the 4H-SiC MOSFET measured via the conventional resonator based EDMR approach and via the wafer-level EDMR approach. Figure 4(a) illustrates the conventional modulated and swept magnetic field resonator-based EDMR of the recombination current in the source-body junction of the n-channel 4H-SiC MOSFETs at an applied forward bias of −2.50 V. The EDMR response here is due to SDR in deep traps (in our case, Si-vacancies) located in the space-charge region of the junction. As mentioned previously, the seminal paper of Kaplan, Solomon, and Mott[23] described the key principles of SDR. The Si-vacancy[27] provides a large EDMR response (S/N ≈ 20/1) in a single sweep measurement of 160 s with a field modulation amplitude of 0.5 mT at 1 kHz. Since this was a resonator-based EDMR measurement, sample preparation for this measurement involved device identification, SiC wafer dicing, silver-paint mounting, and wire-bonding to the device contact pads. This preparation is required for *every* device investigation utilizing the conventional sample-in-resonator EDMR approach. The simplification of the wafer-level non-resonant EDMR approach presents huge advantages in device investigations. While the reliability and performance limiting nature of the Si vacancy defect shown in Fig. 4(a) are of real interest, we have

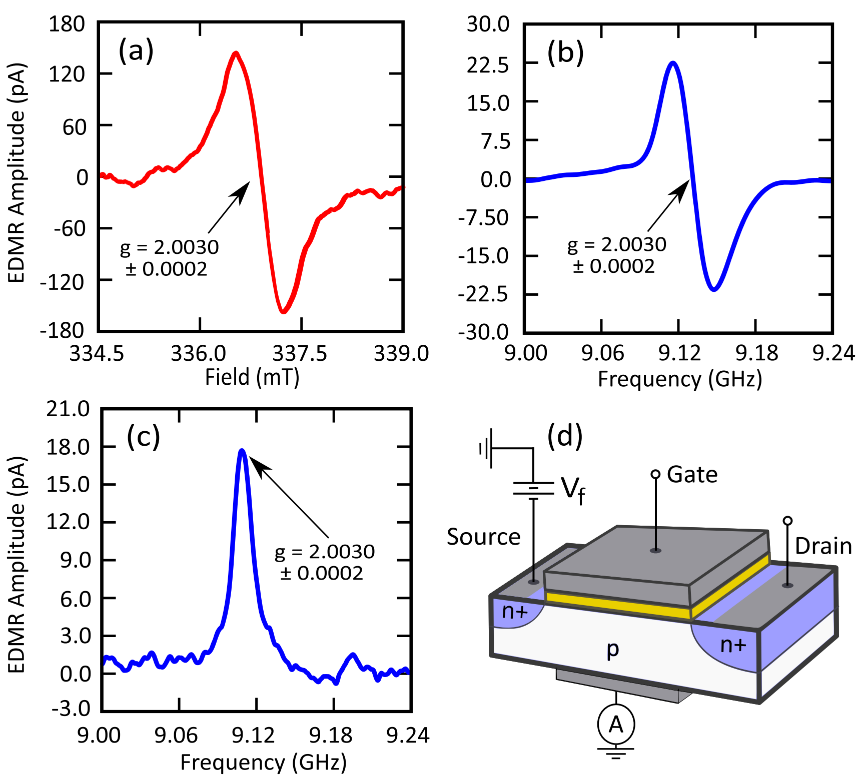

FIG. 4. (a) Conventional magnetic field-swept measurement of the 4H-SiC source-substrate junction, utilizing a cavity-based spectrometer. (b) Frequency swept EDMR measurement of the same junction, with the wafer-level EDMR spectrometer, utilizing FM modulation. (c) Frequency swept EDMR measurement of the same junction, with the wafer-level EDMR spectrometer, utilizing AM modulation. (d) A cartoon illustration of the biasing characteristics for the EDMR measurements made above. The source to body junction is forward biased and the recombination current is measured in the depletion region of this p-n junction. Reprinted with permission from McCrory *et al.*, IEEE Trans. Device Mater. Reliab. **18**(2), 139 (2018). Copyright IEEE 2018.[32]

chosen to use this defect system as a practical demonstration of the utility of our EDMR measurement approach.

Figure 4(b) shows the wafer-level based X-band frequency swept FM (frequency modulation) detected EDMR response of the source-substrate junction recombination current of the same 4H-SiC MOSFET as used for Fig. 4(a). We again observe the same Si-vacancy defect center (g = 2.0030). In this measurement, the frequency sweep rate was 37 MHz/s, the FM depth was 16 MHz with a lock-in time constant of 0.3 s, and the FM rate was 10 kHz. The total acquisition time was the same (160 s) as in the conventional measurement [Fig. 4(a)]. For this measurement, the input microwave power was 1 mW and the antenna probe was in contact with the surface of the wafer. A direct comparison of frequency and magnetic field swept measurements is relatively straightforward. To facilitate a comparison of the two spectra, we have utilized a conversion factor. From Eq. (1) with g = 2.002 32, 0.1 mT ≈ 2.802 MHz.[25] In principle, a frequency sweep, with a fixed magnetic field, should be identical to a magnetic field sweep, with a fixed frequency, as seen in Eq. (1). A comparison of the cavity based measurement [Fig. 4(a)] to the wafer-level measurement [Fig. 4(b)] yields a comparable response in terms of S/N.

In EPR, AM (amplitude modulation) detection is sometimes employed to reduce the experimental burden of large modulation depths needed to resolve broader spectral line widths.[25] The non-resonant frequency swept EDMR approach is also amenable to AM detection. This is demonstrated for the same Si-vacancy defect [Fig. 4(c)]. The expected absorption-like line shape was resolved using 90% modulation depth, meaning that the microwave power is modulated from 100% down to 10% of the total power at the same modulation frequency utilized in the previous FM sweep [illustrated in Fig. 4(b)]. A direct comparison is difficult to make with AM detection because our conventional EDMR spectrometers do not have AM capabilities. However, it appears that the signal to noise is comparable with the FM frequency swept detection. Demonstration of frequency swept EDMR measurements detected in an experimentally advantageous manner with no additional sample preparation serves as proof of the validity of this technique. In the Bipolar amplification effect, Spin dependent charge pumping, Rapid frequency scan EDMR, and Spatially resolved EDMR sections we demonstrate the utility of this approach by examining the Si-vacancy defect participation in a variety of other spin dependent currents in these devices.

Bipolar amplification effect (BAE)

The SDR current demonstrations above provide information about deep level defects in the depletion region of source to channel junctions. A variant on this measurement's biasing scheme can shift the focus from the junction to the channel region.[21] In this approach, the transistor is biased in the sub-threshold regime such that the source-drain transport current is dominated by near interface recombination events.[21] As the Si-vacancy dominates source to drain current in these MOSFETs,[27] it serves as a good test for this wafer-level non-resonant EDMR measurement. Figure 5(a) illustrates the frequency swept, frequency-modulated BAE measurement on the narrow (250 μm × 4 μm) SiC device. In this measurement, the gate was biased at $V_{th} - V_G$ = 4 V, with −2.9 V on the source electrode while the drain and substrate electrodes where grounded, as illustrated in Fig. 5(b). This signal was acquired in 160 s with an S/N ratio of 100. As discussed previously by Aichinger *et al.*, we observe that the BAE technique can greatly increase the signal to noise ratio of the response.[21]

Spin dependent charge pumping

The SDR current measurements which were shown in Fig. 4 are acquired in a steady state biasing scheme. This biasing scheme yields an SDR current dominated by deep level defects near the middle of the bandgap. In structures such as MOSFETs, technologically important defect levels may exist throughout the entire bandgap. In order to probe a majority of the bandgap, we instead utilize the active biasing scheme of

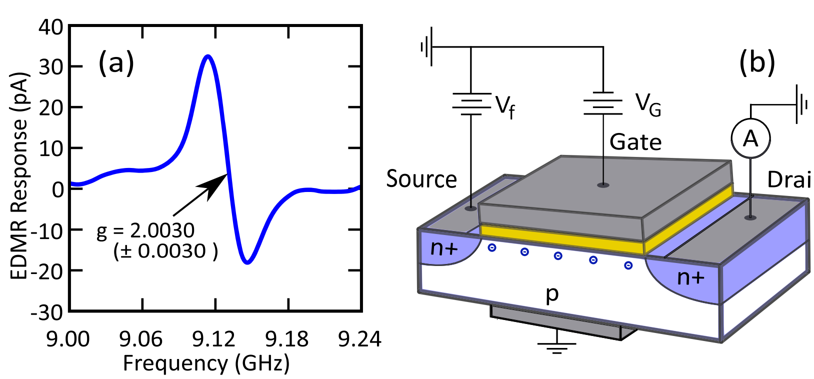

FIG. 5. (a) Frequency swept BAE measurement of the 4H-SiC MOSFET. FM modulation with a depth of 16 MHz; the same as the junction measurements. The BAE response is broader than the junction measurement. (b) The right side of the figure illustrates the BAE biasing scheme on a MOSFET structure. The source is forward biased such that minority carriers are forced into the channel region. Simultaneously, a small bias is applied to the gate, below threshold, such that minority carriers are brought into the channel. This creates a small current flow throughout the device. The drain current is measured with a trans-impedance amplifier and consists of a significant amount of spin dependent recombination current from the interface, as well as the junction regions.

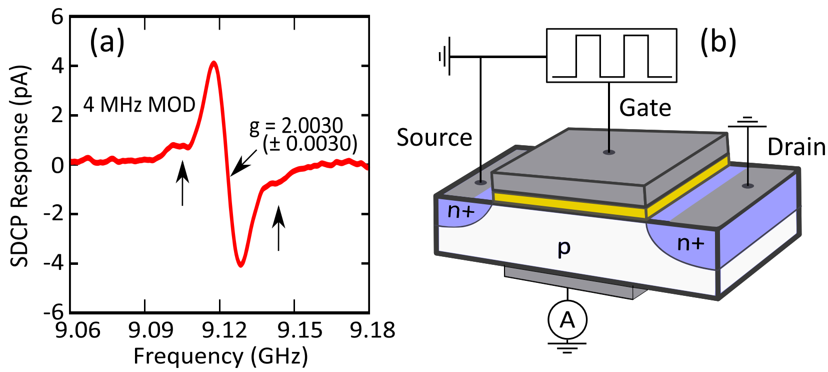

FIG. 6. (a) Frequency swept measurement of the 4H-SiC MOSFET biased with the active SDCP scheme. FM modulation with a depth of 4 MHz. The lower modulation depth helps illuminate possible side peaks. (b) The right side of the figure illustrates the SDCP biasing scheme. The source and drain are grounded while a trapezoidal waveform is applied to the gate contact. This waveform sweeps the MOSFET through accumulation, depletion, and inversion, therefore filling and emptying the interface traps. The spin dependent recombination current is then measured through the body contact via a trans-impedance amplifier.

SDCP. A new square wave trapezoidal waveform, applied to the gate electrode, cycles the device between accumulation and inversion to alternately fill the SiC/SiO_2 interface states with holes and electrons, illustrated in Fig. 6(b). Again, in this biasing scenario, recombination occurs predominately through interface states. Figure 6(a) shows the background-subtracted SDCP detection of the Si-vacancy defect in the narrow (250 μm × 4 μm) SiC device. For this measurement, the gate voltage waveform oscillated between +16 V and −16 V at a frequency of 200 kHz with rise/fall times of 1 μs. Detection utilized FM modulation at a depth of 4 MHz. This signal was acquired in 7200 s with an S/N ratio of ∼50. In the SDCP response, there appears to be two side peaks. Side peaks have previously been observed in 4H-SiC MOSFETs and have been attributed to ^{13}C nuclei in the inner core of the known Si vacancy defect.[3,27] However, the expected response with a ∼2.8 mT separation is quite small and accompanied by two other peaks with a separation of ∼1.3 mT symmetric about the center line. Therefore, we cannot attribute these peaks to nearby ^{13}C nuclei. Similar side peaks have also been attributed to the "10.4 Gauss Doublet."[13,28] The 10.4 Gauss doublet has been definitively linked to hydrogen complexed E′ centers in SiO_2. E′ centers are oxide defects with unpaired electrons residing on a silicon back-bonded to oxygen atoms. It is likely that our observed SDCP side peaks are due to these E′ centers.

Rapid frequency scan EDMR

It has been shown that a significant improvement in S/N can be achieved with rapid-scan detection. This rapid-scan approach has proven quite useful in conventional magnetic field swept EPR[19] as well as in a somewhat protracted frequency swept version.[20] The lack of resonator in our approach opens the bandwidth of detection such that rapid frequency swept measurements can be achieved with some simple alterations in the measurement setup. The rapid-scan measurement setup is schematically shown in Fig. 7. For rapid scan measurements, the conventional microwave source is replaced with a voltage controlled oscillator (VCO) and a voltage-controlled attenuator (VCA). A dual channel arbitrary waveform generator (AWG) is used to control both the VCO and the VCA. Two calibration sequences are performed prior to every measurement to generate (1) the VCO input voltage waveform needed to establish linear frequency sweeps and (2) the VCA input voltage waveform needed to generate a constant power at all frequencies. Any remaining power fluctuations that arise in the EDMR response can also be eliminated via background subtraction. This is achieved by making the EDMR measurement first with the magnetic field within the resonant condition and, then second, by moving the magnetic field significantly off of resonance. Subtraction of these two measurements eliminates any background power fluctuations. Together, this VCO-VCA combination allows for rapid sweeping of large frequency ranges [at least ∼100 GHz/s (∼3.6 T/s)]. However, this sweep rate is purely limited by the gain-bandwidth product of the trans-impedance amplifier used to

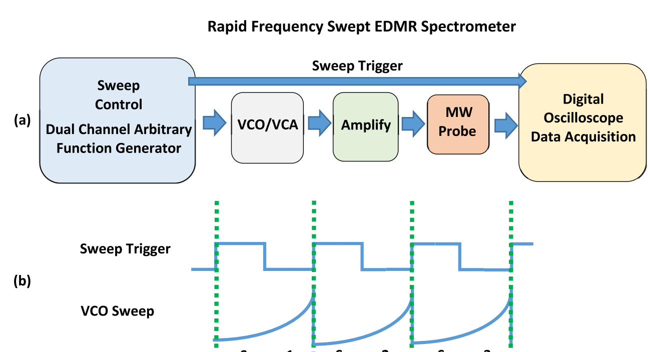

FIG. 7. (a) Rapid frequency swept EDMR spectrometer diagram. The microwave (MW) source is replaced with a voltage controlled oscillator/voltage controlled attenuator (VCO/VCA) combination allowing for rapidly swept GHz frequencies, with flattened power output. (b) Illustration of the triggered VCO/VCA sweep. The VCO/VCA tandem is controlled via a dual-channel arbitrary waveform generator (AWG). This highlights the synced VCO sweep with the sampling oscilloscope, allowing for data averaging. The dashed lines represent the beginning and end of a sweep.

detect the device current. A trans-impedance amplifier with greater gain-bandwidth product would increase the possible sweep rate for this technique.

Conventional data acquisition is no longer viable at these sweep rates due to the high volume of data in short periods of time. Therefore, instead of conventional data acquisition (500 000 kS/s), we instead utilize a high speed digital oscilloscope. The oscilloscope used in these measurements had a sampling rate of 5 GS/s. This allowed for greater sweep rates and greater resolution of our EDMR/EPR spectra. As noted in Figs. 7 and 8, the data acquisition was triggered from the AWG. A gated pulse was sent to the oscilloscope at the beginning of each sweep, ensuring accurate averaging of the data and alignment of the VCO and VCA waveforms. As in conventional EPR, the microwave frequency can be precisely determined (i.e., spectrum analyzer). However, magnetic field calibration via EPR of a spin standard is somewhat more involved for a rapid frequency swept measurement. In general, detection and modulation on the same measurement observable (frequency in this case) poses huge dynamic range issues and normally precludes detection. The situation is somewhat mitigated in our hybrid detection chain seen in Fig. 8. In this approach, the magnetic field is calibrated via observation of the EPR signature of a spin standard. This occurs by switching the detection chain to capture the difference in power diode responses of the non-resonant antenna probe and a "dummy" microwave probe. The dummy microwave probe was created by placing a subminiature A-type connector (SMA) "short" at the end of a SMA coaxial cable with the same length as the non-resonant antenna probe cable. Ideally an identical microwave probe would be used for the dummy probe; however, the short achieved the same desired result. The dummy probe was placed outside of the wafer-level spectrometer, away from the magnetic field. The output of the VCO is amplified with a 15 dBm amplifier and subsequently split (−3 dBm) to both probes. The reflected power is measured from each probe via a Schottky diode attached to the third terminal of a circulator. The difference in reflected power between the two probes is amplified via a differential voltage amplifier and recorded as the frequency is rapidly swept. At resonance, the reflected power from the non-resonant antenna probe will change, while the reflected power from the dummy probe will remain constant. After averaging the rapid frequency swept EPR measurement, the output of the differential amplifier reveals the EPR absorption spectrum. The sensitivity of this approach is limited by the resolution of the VCA to flatten the power for the entire frequency sweep. Since the EPR measurement acts only as a magnetic field marker (no spin counting), this approach is adequate to extract g-values by simply placing a few grains of 2,2-diphenyl-1-picrylhydrazyl (DPPH) on the wafer surface next to the device under EDMR examination. Again, the lone limiting factor in this mode of detection is the bandwidth of the trans-impedance amplifier used to measure the device current, which limits our sweep rate to 100 GHz/s.

Figure 9 shows the rapid frequency scan observations of the Si-vacancy for the same EDMR biasing schemes discussed above. Figure 9(a) illustrates the source-substrate SDR EDMR, Fig. 9(b) depicts BAE EDMR, and Fig. 9(c) shows SDCP EDMR. The trans-impedance amplifier used for Figs. 9(a) and 9(b) was a Femto variable gain high speed current amplifier (DHPCA-100). The gain setting was 10^8 V/A with a bandwidth of 220 kHz, rise time of 1.6 μs, and input noise of 51 fA/$\sqrt{\text{Hz}}$. For Fig. 9(c), we utilized a Stanford Research Systems Current Preamplifier (SR570) with a current gain of 10^6 V/A, a bandwidth of 20 kHz, a bandpass filter between 10 Hz and 1 MHz, an input noise of 1 pA/$\sqrt{\text{Hz}}$, and a rise time of 17.6 μs. The EDMR response of the source-body junction, illustrated in Fig. 9(a), exhibits very high S/N. This "fast-passage" measurement is a technique previously utilized by Cochrane *et al.* to help identify the ^{13}C hyperfine interactions at the Si-vacancy site.[27] Each of these rapid scan acquisitions consist of a 50 000 sweep average, with a sweep rate of 200 sweeps/s. Therefore, each figure took about 4.5 min to acquire. In comparison to the modulated results, we notice that there is a significant increase in the background of the EDMR response. In order to improve the S/N of the response, we increased the sweep rate. However, with increased sweep rates, (>100 GHz/s) we observe a significant decrease in amplitude as well as broadening of the EDMR response. This is mostly due to the limited gain-bandwidth product of our trans-impedance amplifier.

A limiting factor for rapid-scan measurements is the bandwidth of the current amplifier. The bandwidth limits the

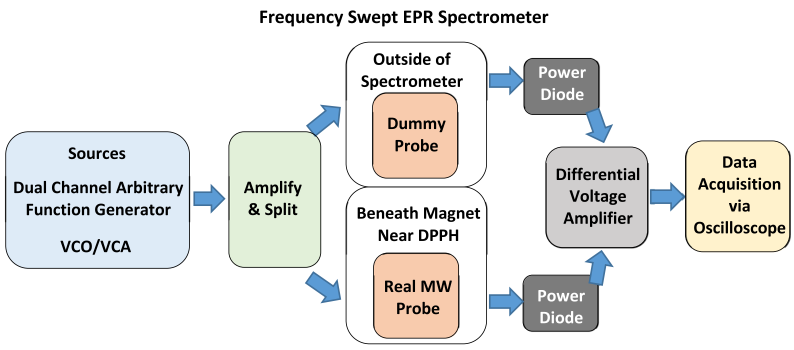

FIG. 8. Frequency swept EPR spectrometer diagram. The same VCO/VCA combination is utilized allowing for rapidly swept GHz frequencies, with flattened power output. The VCO/VCA tandem is controlled via a dual-channel AWG. That output is amplified and split and sent to two different probes. One "Real Probe" lies next to the spin standard beneath the magnet, while the other is separate from the system. The reflected power from each probe is measured (via a power diode attached to the third terminal of a circulator), and their difference is amplified and plotted. This method enhances the EPR measurement. It is important to note that this method is only sensitive enough for field-calibration measurements.

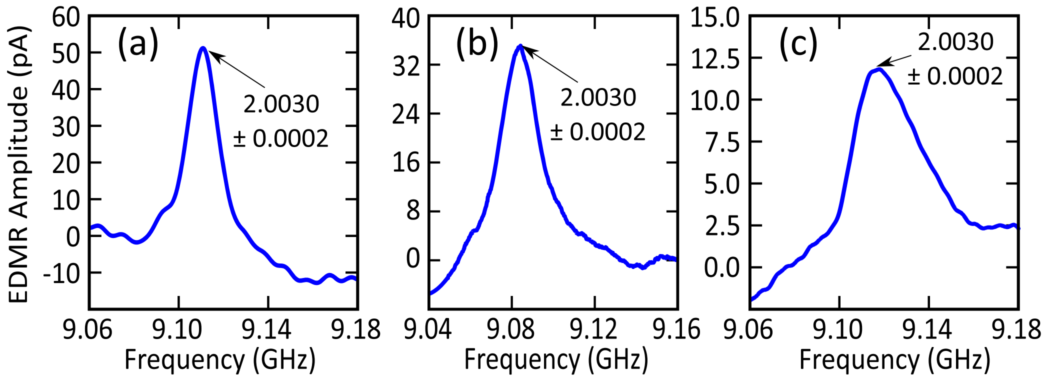

FIG. 9. (a) Rapid frequency swept EDMR of the source-body junction at a fixed magnetic field of 324.9 mT. (b) Rapid frequency swept EDMR utilizing the BAE biasing scheme of the same 4H-SiC MOSFET at a fixed magnetic field of 324.0 mT. (c) Rapid frequency swept SDCP EDMR of the same 4H-SiC MOSFET at a magnetic field of 325.1 mT. The resonance frequency shift is likely due to temperature fluctuations (these measurements were made a different times throughout the year) and/or slight variations in the device under test and magnet position.

speed with which we can make measurements (~100 GHz/s), as well as the potential S/N. Enhancements to the amplifier would allow for faster scan rates and more insight into fast-passage effects, which is a powerful tool for elucidating hyperfine interactions. Rapid frequency swept EDMR has the potential to enhance the S/N of EDMR measurements and reduce the overall measurement time. The non-resonant EDMR probe is extremely useful because it enables seamless switching between rapid-frequency swept measurements and conventional modulated measurements.

Spatially resolved EDMR

Thus far, we have demonstrated the validity and utility of the non-resonant microwave probe based wafer level EDMR. In each case, the antenna probe is held at a fixed position relative to the device. However, one of the assets of this approach is the ability to laterally vary the position of the antenna probe such that one can profile the EDMR response across the device. Spatially resolved EDMR was first demonstrated by Sato *et al.*[29] and Katz *et al.*[30] by utilizing magnetic field gradients that were swept across the device under test. This allowed for spatial tuning of the exact resonance condition, with resolution in millimeters and tens of microns. Our technique utilized the maneuverability of the antenna probe to fix the location of the impending B_1.

This effect was demonstrated by monitoring the EDMR response of a 100 μm × 100 μm MOSFET, biased with the DCIV[31] biasing scheme [Direct-Current I (as in current) – V (as in voltage)]. The widely utilized DCIV biasing scheme is a measurement of the recombination current of a gated diode and, in our case, a MOSFET. The MOSFET source-channel and drain-channel junctions are slightly forward biased as the current is measured at the substrate contact. As the gate voltage is swept from inversion to slight accumulation, a significant portion of the substrate current is due to recombination and is inherently spin dependent. Therefore, the DCIV biasing scheme allows for EDMR detection within the MOSFET

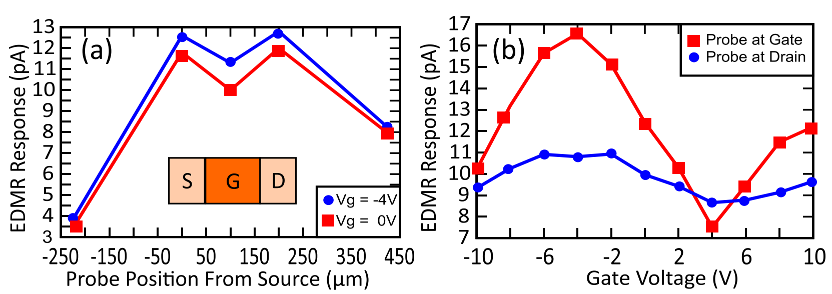

FIG. 10. (a) SDR amplitude versus non-resonant microwave probe position. The measurements were made at two different gate biases: V_g = 0 V and V_g = −4 V. V_g = −4 V corresponds to the gate bias in which the maximum SDR was observed. A cartoon depiction of the 4H-SiC n-MOSFET is overlaid on the plot and corresponds to the actual position of the MOSFET relative to the probe position on the x-axis. (b) illustrates the SDR amplitude with the microwave probe placed at two different locations, above the gate and above the drain region. A significant increase in the response is measured when the probe is placed above the gate and the gate bias is swept through the peak DCIV voltage.

channel and junction regions. Figure 10(a) illustrates a change in the EDMR amplitude as the non-resonant microwave probe is scanned across the MOSFET. The EDMR response peaks near the junctions and decreases as the probe is moved away from the MOSFET. The overall response increases with the appropriate DCIV gate bias. It is important to note that the EDMR profiling is dependent upon the fine control of the micromanipulator and the size of the microwave probe. Figure 10(b) illustrates the EDMR response versus DCIV gate bias with the probe seated at the gate and also seated at the drain. The peak response occurs when the probe is located at the gate, with a DCIV V_G = −4 V. The response at the same biasing conditions is much smaller when the probe is located at the drain. The location of the probe has a sizeable impact on the EDMR response. In summary, this somewhat crude demonstration of spatial profiling provides proof of concept evidence that such spatial dependence studies can proceed in this manner. However, it could be enhanced by decreasing the probe size and decreasing the output B_1 to reduce the volume of the probed region.

CONCLUSIONS

The incorporation of an EDMR spectrometer into a semiconductor wafer-probing station brings the power and sensitivity of EDMR to the ease-of-use of a wafer-probing station. We have demonstrated the utility of a wafer-level EDMR spectrometer by analyzing the SDR current within a 4H-SiC n-MOSFET. The wafer-level setup allowed for quick transition between different biasing schemes such as BAE and SDCP. Rapid-frequency swept SDR, BAE, and SDCP were performed. These measurements demonstrate the advantages of a wide-bandwidth non-resonant microwave probe. Finally, the demonstration of spatially resolved EDMR illustrates another potential advantage of the newly developed microwave probe. We believe that this wafer-level EDMR spectrometer could be extremely useful for the semiconductor research and development community.

ACKNOWLEDGMENTS

Funding for this work was provided through the National Institute of Standards and Technology (NIST). Travel grants were provided by the EPR Technology Transfer Experience (ETTE) via SharedEPR, an NSF funded organization. This work was supported in part by the Air Force Office of Scientific Research under Award No. FA9550-17-1-0242 and in part by the US Army Research Laboratory, Adelphi, MD.

Certain commercial equipment, instruments, or materials are identified in this paper in order to specify the experimental procedure adequately. Such identification is not intended to imply recommendation or endorsement by the NIST nor is it intended to imply that the materials or equipment identified are necessarily the best available for the purpose.

REFERENCES

[1] C. J. Cochrane, P. M. Lenahan, and A. J. Lelis, J. Appl. Phys. **105**, 064502 (2009).
[2] C. J. Cochrane, P. M. Lenahan, and A. J. Lelis, Appl. Phys. Lett. **90**, 123501 (2007).
[3] M. A. Anders, P. M. Lenahan, C. J. Cochrane, and A. J. Lelis, IEEE Trans. Electron Devices **62**, 301 (2015).
[4] D. J. Meyer, P. M. Lenahan, and A. J. Lelis, Appl. Phys. Lett. **86**, 023503 (2005).
[5] M. J. Mutch, P. M. Lenahan, and S. W. King, J. Appl. Phys. **119**, 094102 (2016).
[6] C. Boehme, J. Behrends, K. V. Maydell, M. Schmidt, and K. Lips, J. Non-Cryst. Solids **352**, 1113 (2006).
[7] K. Lips, C. Boehme, and W. Fuhs, IEE Proc., Circuits, Devices Syst. **150**, 309 (2003).
[8] D. R. McCamey, H. Huebl, M. S. Brandt, W. D. Hutchison, J. C. McCallum, R. G. Clark, and A. R. Hamilton, Appl. Phys. Lett. **89**, 182115 (2006).
[9] P. M. Lenahan and M. A. Jupina, Colloids Surf. **45**, 191 (1990).
[10] J. W. Gabrys, P. M. Lenahan, and W. Weber, Microelectron. Eng. **22**, 273 (1993).
[11] J. P. Campbell and P. M. Lenahan, Appl. Phys. Lett. **80**, 1945 (2002).
[12] J. T. Ryan, P. M. Lenahan, T. Grasser, and H. Enichlmair, Appl. Phys. Lett. **96**, 223509 (2010).
[13] M. A. Anders, P. M. Lenahan, and A. J. Lelis, J. Appl. Phys. **122**, 234503 (2017).
[14] C. Boehme and K. Lips, Phys. Rev. B: Condens. Matter Mater. Phys. **68**, 245105 (2003).
[15] J. J. L. Morton, A. M. Tyryshkin, R. M. Brown, S. Shankar, B. W. Lovett, A. Ardavan, T. Schenkel, E. E. Haller, J. W. Ager, and S. A. Lyon, Nature **455**, 1085 (2008).
[16] A. Morello, J. J. Pla, F. A. Zwanenburg, K. W. Chan, H. Huebl, M. Mottonen, C. D. Nugroho, C. Yang, J. A. van Donkelaar, A. D. C. Alves, D. N. Jamieson, C. C. Escott, L. C. L. Hollenberg, R. G. Clark, and A. S. Dzurak, Nature **467**, 687 (2010).
[17] F. Klotz, H. Huebl, D. Heiss, K. Klein, J. J. Finley, and M. S. Brandt, Rev. Sci. Instrum. **82**, 074707 (2011).
[18] J. P. Campbell, J. T. Ryan, P. R. Shrestha, Z. Liu, C. Vaz, J. H. Kim, V. Georgiou, and K. P. Cheung, Anal. Chem. **87**, 4910 (2015).
[19] J. W. Stoner, D. Szymanski, S. S. Eaton, R. W. Quine, G. A. Rinard, and G. R. Eaton, J. Magn. Reson. **170**, 127 (2004).
[20] M. Tseitlin, A. Dhami, R. W. Quine, G. A. Rinard, S. S. Eaton, and G. R. Eaton, Appl. Magn. Reson. **30**, 651 (2006).
[21] T. Aichinger and P. M. Lenahan, Appl. Phys. Lett. **101**, 083504 (2012).
[22] B. C. Bittel, P. M. Lenahan, J. T. Ryan, J. Fronheiser, and A. J. Lelis, in *2011 International Semiconductor Device Research Symposium* (IEEE, 2011), p. 142.
[23] D. Kaplan, I. Solomon, and N. F. Mott, J. Phys. Lett. **39**, 51 (1978).
[24] G. Kawachi, C. F. O. Graeff, M. S. Brandt, and M. Stutzmann, Jpn. J. Appl. Phys., Part 1 **36**, 121 (1997).
[25] C. P. Poole, *Electron Spin Resonance: A Comprehensive Treatise on Experimental Techniques* (Courier Corporation, 1996).
[26] H. Hirata, T. Walczak, and H. M. Swartz, J. Magn. Reson. **142**, 159 (2000).
[27] C. J. Cochrane, P. M. Lenahan, and A. J. Lelis, Appl. Phys. Lett. **100**, 023509 (2012).
[28] C. J. Cochrane, P. M. Lenahan, and A. J. Lelis, J. Appl. Phys. **109**, 014506 (2011).
[29] T. Sato, H. Yokoyama, H. Ohya, and H. Kamaday, J. Magn. Reson. **153**, 113 (2001).
[30] I. Katz, M. Fehr, A. Schnegg, K. Lips, and A. Blank, J. Magn. Reson. **251**, 26 (2015).
[31] C. J. Cochrane, P. M. Lenahan, and A. J. Lelis, in *IEEE International Integrated Reliability Workshop Final Report* (IEEE, 2008), p. 68.
[32] D. J. McCrory, M. A. Anders, J. T. Ryan, P. R. Shrestha, K. P. Cheung, P. M. Lenahan, and J. P. Campbell, IEEE Trans. Device Mater. Reliab. **18**(2), 139 (2018).